Proceedings of the 9th Biennial ASME Conference on Engineering Systems Design and Analysis
ESDA08
July 7-9, 2008, Haifa, Israel

ESDA2008-59373

AN INVESTIGATION INTO EFFECT OF TRAIN CURVING ON WEAR AND CONTACT STRESSES OF WHEEL AND RAIL

Xuesong Jin*
State Key Laboratory of Traction Power

Jun Guo
State Key Laboratory of Traction Power

Xinbiao Xiao
State Key Laboratory of Traction Power

Zefeng Wen
State Key Laboratory of Traction Power

Southwest Jiaotong University, Chengdu 610031, China

ABSTRACT

Some important papers concerning the studies on rail wear and wheel/rail contact stresses are reviewed. The present paper utilizes a numerical method to analyze the effect of railway vehicle curving on the wear and contact stresses of wheel/rail. The numerical method considers a combination of Kalker's non-Hertzian rolling contact theory, a material wear model and a vertical and lateral coupling dynamics model of a half vehicle and a curved track. The present analysis investigates the influence of the curving speed, the curved track super-elevation and the rail cant on the wear and the contact stresses. Through the detailed numerical analysis, it is found that the maximum contact stress depends greatly not only on the curving speed but also on the profiles of the wheel/rail. The curving speed increasing leads to increase the normal load of the wheel rolling over the high curved rail, but, decrease the normal contact stress level under the condition of the optimum match of wheel/rail profiles. The track super elevation increasing efficiently lowers the contact stresses and the wear at a constant curving speed. The rail cant has a great influence on the low rail wear of the curved track. Increasing the rail cant leads to the great growth of the low curved rail wear, the reduction in the high rail wear. The results are very useful in the maintenance of the track.

1. INTRODUCTION

The wear and rolling contact fatigue of wheels and rails cost China railways about 110 millions US dollars per year. The wear and fatigue occur predominantly on sharp curved tracks, joint rails and turnouts [1,2]. When a wheel rolls over a rail with a large slide, a large amount of material on the wheel or the rail running surface is removed due to high contact stresses and high temperature [3]. Severe wear causes the great change of rail profile, therefore, strongly affects the behaviour of running railway vehicles, such as motion stability, riding comfort and derailment safety. The wear amount and the present shape of the rail in service are the key criteria for rail replacement in the rail industry. However, the wear is often utilized to extend the use life of the rails which have small cracks on their running surfaces at railway sites. As well known, cracks and wear are two types of rail damage. Proper wear rate occurring on the rail running surface is able to eliminate small existing cracks or suppress the growth of existing cracks efficiently [4]. According to the mechanism many railway companies on the world developed the optimum techniques of rail grinding [5-7]. For instance, MRS in Brazil applied the advanced technique of rail grinding to the maintenance of the heavy haul track, and the use life of rails used in the heavy haul lines increased doubly [8]. Therefore, railway companies are much concerned with the studies and treatment of rail wear. Rail wear studies are very complicated, and involve many subjects, such as structural coupling dynamics of railway vehicle and track, rolling contact mechanics, tribology, metallurgy, and numerical method.

In the past, many papers on wear and contact stresses of wheel/rail were published. In 1976, using Amsler testing machine of two rollers, Bergley made an investigation into the wear of wheel flanges against the sides of the rails, caused by rolling/sliding contacts sustaining high cyclic stresses at low slide/roll ratios [9]. He concluded that the severe wear of contacts at low slide/roll ratios is caused by high resolved cyclic stresses that result in continual plastic deformation of the surface layers. Using the same testing facility, three wear regimes of wheel/rail steels in rolling/sliding contact were identified by Bolton and Clayton et al. [10,11]. The characteristic of wear modes within these regimes, referred to

* Professor and author of correspondence

as types I, II and III, was determined through metallurgical examination. Relations between the wear rates and test contact parameters, for wear types I and II, can be presented by mathematical expression. It was found that the wear modes occurred in side-worn rail on curved track correlated with laboratory wear types II and III to the extent that the laboratory test offers a prediction of the wear status of rail in service [12]. Tyfour et al. [13] made an investigation into the steady state wear behaviour of pearlitic rail steel after a certain number of rolling-sliding cycles through test in detail. Also the effect of strain hardening and unidirectional plastic strain accumulation on the wear behavior was studied. The test result showed that the start of the steady state wear rate coincides with the cessation of plastic strain accumulation and additional strain hardening, namely, the steady state wear rate is established when the material with the same history of strain hardening and accumulated unidirectional plastic strain reaches the surface and the unidirectional plastic strain limit to failure is reached. In their results it was found that the rates of strain accumulation and strain hardening present maxima at the beginning of the rolling/sliding process, and decrease in non-linear fashion to stop after a certain number of cycles. Muster et al. [14] observed and analyzed the effect of different grades of rail steel in service on the resistance to wear and fatigue damage. Tournay et al. [15] analyzed the transition from the wear to stress regime of the rails in service. They found that tighter gauge tolerances, rail crown grinding producing tighter contact bands and improved vehicle tracking properties have concentrated contact on the wheel tread enhancing hollow wear band. Since the lateral excursions of the wheelset often occur outside the hollow wear band, small contact areas, high contact stresses and large longitudinal creepages as s result of the large instant radius difference generated on the wheelsets often form. This can cause high longitudinal material flow, shelling and checking in the rails. Ueda et al. [16] clarified the effects of carbon content on the rolling contact wear in steels through a two-cylinder rolling contact wear test using pearlitic steels with a carbon content ranged from 0.8 to 1.0 mass%. They obtained conclusions as follows: (1) the wear resistance of pearlitic rail steels improves as carbon content and rolling contact surface hardness increase, and the rolling contact surface hardness is a main factor affecting the wear; (2) the rolling contact surface hardness increases due to raising the working-hardening rate of the rolling contact surface as carbon content increases. That is because an increase in the cementite density increases the amount of dislocation in the matrix ferrite and promotes the grain refinement of the matrix ferrite. Therefore, the matrix ferrite is strengthened. Through experimental examinations of the tractive rolling contact between rail and wheel using two-roller test machine [17], Deters et al. found that the wear volume rise turned out to be proportional to the increase of the acting pressure and the creepage between the two rollers. An increase in the circumferential speed of the test rollers caused a reduction in the wear volume. A significant wear decrease at the driven roller modeling rail could be achieved by periodically reversing the direction of the acting traction force.

Actually, the wear and rolling contact fatigue of wheel/rail depend greatly on their profiles and contact surface status, the geometry sizes of track and dynamical behavior of railway vehicle coupled with the track. Their numerical analysis needs the power and efficient numerical method considering the factors mentioned above. Such a numerical method can help identify the risk of severe or catastrophic wear resulting from increased train speeds and axle loads, and determine more efficient maintenance schedules for track and rolling stock [18]. Shen et al. [19] numerically analyzed the influence of rail lubrication on freight car wheel/rail wear rates. Their numerical model considered a C60 freight car of China with two sets of standard 3-piece trucks called “TRUCK 8” under the condition of steady-state curving through a rigid curved track. The steady-state curving indicates the accelerations of the system in the calculation were neglected. Only the equations for a single-track/half-car body were solved in order to reduce the numerical computation. Rail lubrication was simulated through changing friction coefficient between the wheels and rails. The non-linear creep forces in the Hertzian elliptical contact areas of the wheels/rails were calculated with the model put forward by Shen et al. [20]. The numerical results indicated that for the curved tracks with radii less than 400 m, the wheel/rail wear rate under lubrication may be reduced to 40% of that without lubrication. Jendel [21] developed a wheel profile wear prediction tool based on a load collective concept, where time-domain dynamics simulation of the vehicle coupled with track was carried out based on actual track data, measured rail profiles as well as pertinent conditions. In Jendel’s calculation model, the vehicle model consisted of a full dynamic rigid multi-body model with a car-body, two bogie frames and four wheelsets connected by linear and non-linear suspension elements. The track was modeled as a mass following each wheelset with a degree of freedom in the lateral direction. Archard’s wear model was used to calculate the material removal due to wear [22]. To verify the prediction tool, they made comparisons between simulated and measured wheel profiles for a total running distance of about 200,000 km, as well as between four scalar wear measures: flange thickness, flange height, flange inclination and the decrease in area between successive profiles. The comparisons showed a good agreement. Ref. [23] declared a method for the computation of the rail surface degradation in a curved track where the major surface degradation phenomenon is actually a combination of wear and plastic deformation. In the numerical analysis of the wheel/rail in rolling contact, the normal pressure was calculated with the modified Winkler method [24], and calibrated with the results obtained by FEM modeling of the wheel/rail in contact with elastic/plastic deformation [25]. A tangential Winkler model that includes the effect of neighboring cells was used to calculate the elastic tangential stress and displacement field. In Archard’s wear model used to calculate the material removal due to wear, the friction coefficient and wear coefficient were

determined in advance using pin on disk tests [26]. Two point contacts occur easily between the leading wheelsets and the high rails of sharp curved track during the curving of trains. Such two point contacts cause severe side-wear of the rails. So, a typical two-point contact in a sharp curve was analyzed and discussed by Telliskivi et al. [26]. Enblom et al. [27] analyzed the wheel profile development due to wear-influence of disc braking and contact environment. Their wear prediction model is the same as that Jendel used. Magel et al. [28] evaluated the comparative wear performance of the new proved profile wheel against existing wheels through a numerical simulation of the wheel-rail interaction over 800 km of running by using a quasi-static curving model that was validated through a comparison with NUCARS predictions. Their prediction showed that the proved profile wheel reduced wheel flange wear by at least 25% when compared to the existing Amtrak Standard wheel profile. Paper [29] presents a numerical procedure for design of wheel profiles based on the function of rolling radii difference of left and right wheels of wheelset. Using the procedure the obtained new wheel profile can reduce wheel/rail wear without loss of the vehicle dynamic performance, which is validated through the analysis using ADAMS/Rail computational software.

In the present study, a numerical method is used to investigate the influence of railway vehicle curving on rail wear and wheel-rail contact stresses. The method considers Kalker's three-dimensional rolling contact theory with non-Hertzian form, a material wear model, the vertical and lateral coupling dynamics of a half railway vehicle and a curved track, and the contact geometry calculation of wheelset and track. Kalker's rolling contact theory [30] is introduced and modified [31] to calculate the frictional work density and the contact stresses in the contact areas between the wheels and rails. The frictional work density is defined as the frictional work per unit area. The material wear volume is calculated with the linear model of material wear related to the frictional work density [32, 33]. A half railway vehicle coupled with a complicated physical model of the track is considered in the dynamics simulation. The half vehicle has a two-axle bogie and doubled suspension systems. It was treated as a full dynamic rigid multi-body model. The model of the track by Zhai et al. [34] is introduced in the present work.

2. CALCULATION MODEL

2.1. General Descriptions

Curved rail wear depends greatly on the profiles, materials and contact surface status of wheel and rail, train curving speed, and dynamical characteristics of railway vehicle and curved track. Under a given wheel load, the profiles and surface status of wheel and rail determine the wheel/rail contact stresses which affect rail wear. Severe rail wear changes the behavior of wheel and rail in rolling contact and deteriorate railway vehicle tracking performance. The larger normal load and creep forces generate between the wheel and rail. The contact stresses, therefore, become larger. Such a situation easily destroys vehicles and track, especially, severe damage occurs on the running surfaces of wheel and rail. The vehicle curving behavior is intimately related to the dynamical characteristics of the vehicle and the track. In addition, the physical properties of wheel and rail materials much affect the rate of material wear and crack growth on the rail running surface. The influences of the above factors are strongly coupled. A comprehensive model accounting for these factors is necessarily developed to predict the profile degradation of rail due to wear and fatigue.

The present model is roughly depicted in Fig. 1 according to the above brief discussion on these factors. In Fig. 1 Y_{wi} and Ψ_{wi} are, respectively, the lateral displacement and yaw angle of wheelset i, subscripts i =1, 2 denote the leading and trailing wheelsets considered in the calculation model, respectively, Y_{rk} is the lateral displacement of the rail head under wheel k, and subscript k is the number of the wheels in the model, δ_k and h_k are, respectively, the contact angle and the normal distance or normal gap between wheel k and the rail at the contact point of the wheel/rail. The selected ranges for i and k depend on the total numbers of the wheelsets in the calculation model. ξ_{jk} and P_{wrzk} are, respectively, the creepages and the vertical loads between the wheels and the rails, subscripts j=1, 2, 3 indicate, respectively, the longitudinal, lateral and spin creepages, subscripts w and r denote, respectively, wheel and rail, z indicates the vertical direction of the track. f_{wk} denotes the frictional work density in the contact area under wheel k. Figure 1 indicates a feedback process between the transient coupling dynamics of the vehicle and the curved track and long-term wear processes. In the analysis, a coupling dynamics model of the railway vehicle and the curved track is used to analyze the dynamical behavior of the vehicle and the track. Through the dynamics analysis, ξ_{jk}, P_{wrzk}, Y_{wi}, Ψ_{wi} and Y_{rk} are obtained. Using the calculation model of wheel-rail contact geometry briefly discussed in the present paper later, and known Y_{wi}, Ψ_{wi} and Y_{rk}, h_k and δ_k are found. ξ_{jk}, P_{wrzk}, h_k and δ_k will be used in the rolling contact calculation of the wheel/rail using Kalker's rolling contact theory. Through the rolling contact calculation, we obtain f_{wk}, the contact stresses, stick/slip

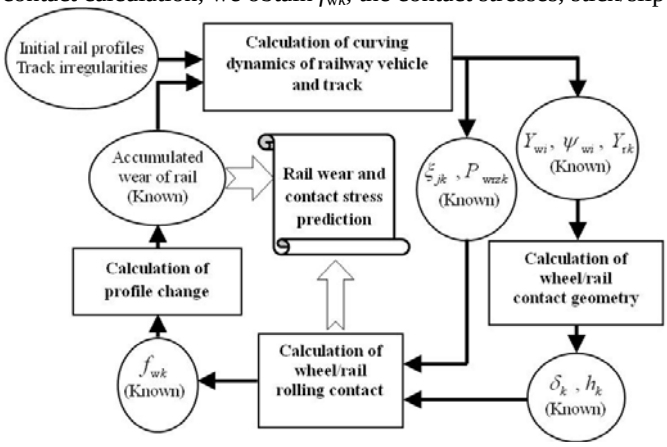

Figure 1. A general description of curved rail wear model

areas, the wear volume, etc. Kalker's model of three dimensional elastic bodies in rolling contact was modified [31] and is introduced in such a rolling contact calculation of the wheel/rail systems where the effect of the rail profile change on the dynamics and the contact stresses is considered. If the frictional work density on the contact area is known, the wear depth on the running surface is determined using the material wear model by Clayton et al. [32, 33]. Using the known wear depth at the present step, the existing rail initial profile can be updated for the next loop calculation. After such repeated loop calculations the accumulated material wear and its distribution on the rail head are obtained. In each step calculation, the contact stresses, the stick/slip areas, the slip distribution in the contact area, etc are also determined.

It should be noted that for the introduced rail wear model, the effect of material working-hardening due to repeat rolling and press of wheels on the wear is neglected.

2.2. Model of Railway Vehicle and Curved Track

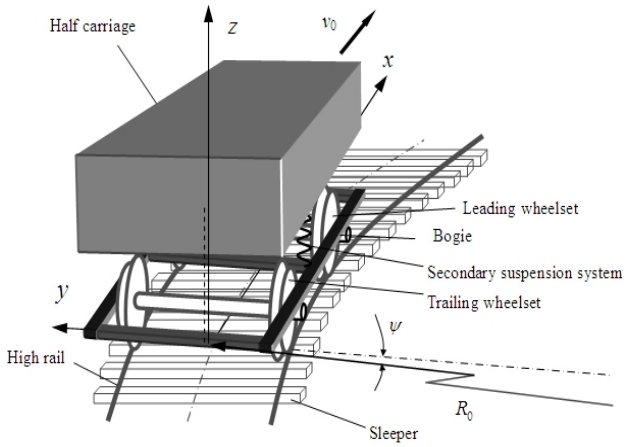

Figure 2. A half vehicle passing through a curved track

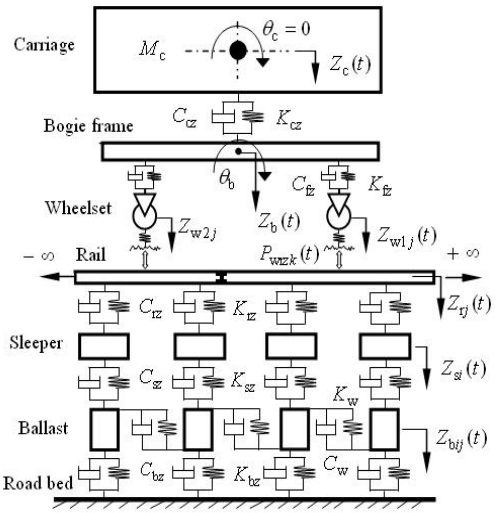

Figure 3. Elevation of a half passenger car coupled with a curved track

At railway sites, severe rail wear and damage, usually, occur at sharp curved tracks. In the present model of railway vehicle and track, a half vehicle and a curved track with radius R_0=800 m, are taken into consideration, as shown in Fig. 2. Figure 2 illustrates the half railway car passing through the curved track. In Fig. 2, ψ indicates the yaw angle of wheelset, v_0 denotes the curving speed, and R_0 is the radius of the curved track. The curved track has the circle curve length l_c=200 m, the transient curve length l_{ct}=120 m, the track gauge d_t=1435 mm, and the sleeper pitch l_0=600 mm. The super-elevation h_t=120, 150, and 180 mm, the rail cant α_t=1/20, 1/30, and 1/40, v_0=80, 100, and 120 km/h are respectively considered. The calculation model of the half vehicle and the curved track, as shown in Fig. 2, is described with Fig. 3. The figure just illustrates the side view of the half vehicle coupled with the track. Their end view was given in Refs. [35,36].

2.2.1. Vehicle model description

From Fig. 3 it is obvious that the half vehicle is treated as a full dynamic rigid multi-body model. The variables Z and θ with subscripts indicate, respectively, the vertical displacement and the pitching angle of the components of the vehicle. K and C with subscripts stand for the coefficients of the equivalent spring stiffness and the equivalent damper, respectively. The equivalent springs and the equivalent dampers are used to replace the connections between the components of the half vehicle and the curved track. M_c is the mass of the half carriage. In order to show the numerical results clearly and conveniently, the left and right wheels of the leading wheelset are numbered 1 and 2, respectively, and the corresponding wheels of the trailing wheelset numbered 3 and 4. The leading and trailing wheelsets are numbered 1 and 2 respectively. It should be noted that since the half vehicle is considered in the dynamics analysis it cannot be balanced when its running simulated on the track. Therefore, the pitching and the yaw motion of the carriage have to be neglected, namely, let θ_c=0 always, as shown in Fig. 3, and ψ_c=0. ψ_c indicates the yaw angle of the carriage that is not shown in Figs. 2 and 3. The accelerations of the centers of all the components of the half vehicle are assumed to be zero in the longitudinal direction. The flexibility of the components of the vehicle is ignored.

2.2.2. Track model description

The track, except for the rails, is also treated as a dynamic rigid multi-body model. The calculation model of the track used in Ref. [34] is introduced in the present paper. Due to considering the half vehicle passing through the curved track, the four wheels of the same bogie interact with the two side rails of the track through the axles and the rails.

Each rail is modeled by an Euler beam. The calculation length of the rail is 36 m. The two ends of the rails are hinged. The vertical and lateral bending deformations and rotation of the rails are taken into account. The longitudinal deformation and the cross influence of the vertical and lateral bending and rotational deformations of the rails are ignored. Using the

Rayleigh-Ritz method the fourth-order partial differential equations of the rail are converted into second-order ordinary equations [35, 36]. The second-order ordinary equations are constituted based on the superposition principle of beam theory. The modal shape functions from the first to the 120th are used.

The sleepers are treated as rigid bodies accounting for the vertical, lateral and roll motions of them only. The ballast bed is replaced with equivalent mass bodies. The connection of the neighboring mass bodies is replaced with an equivalent spring and an equivalent damper, as shown in Fig. 2. Only the vertical motion of them is taken into consideration. The motion of the substrate is neglected. The equivalent springs and dampers are used to replace the connections from the rails to the subgrade.

2.2.3. Model of wheel-rail contact

In the analysis of the transient coupling dynamics of the vehicle and the curved track, an accurate and quick calculation model of coupling of the wheel-rail system is needed. The calculation model of wheel-rail coupling, usually, includes the normal and tangential contact problems. Considering the influence of the wear of the rail running surface on the normal load, the usual model of the wheel-rail normal load reads

$$P_{\mathrm{w}rnk}(t)=\begin{cases} C_{\mathrm{H}}[Z_{\mathrm{w}nk}-Z_{\mathrm{r}nk}+\delta_0-U_{\mathrm{w}k}]^{3/2}, \\ \qquad Z_{\mathrm{w}nk}-Z_{\mathrm{r}nk}+\delta_0-U_{\mathrm{w}k}>0 \\ 0, \\ \qquad Z_{\mathrm{w}nk}-Z_{\mathrm{r}nk}+\delta_0-U_{\mathrm{w}k}\le 0 \end{cases} \tag{1}$$

where k=1, 2, 3 and 4 indicate wheels 1, 2, 3 and 4, respectively, $Z_{\mathrm{w}nk}$ and $Z_{\mathrm{r}nk}$ are the normal displacements of wheel k and the rail at their contact point, and they are determined by solving the system equations and calculating the contact geometry of the wheelset and the track. δ_0 is the approach between the wheel and rail caused by the static normal load when the vehicle is on the central line of the track. $U_{\mathrm{w}k}$ is the depth of the accumulated wear on the rail running surface, at the contact point of wheel k and the rail. It should be noted that the model of the normal contact load is approximately described with a Hertzian contact spring with a unilateral restraint. In (1), $Z_{\mathrm{w}nk}-Z_{\mathrm{r}nk}+\delta_0-U_{\mathrm{w}k}>0$ indicates the wheel-rail in contact, and $Z_{\mathrm{w}nk}-Z_{\mathrm{r}nk}+\delta_0-U_{\mathrm{w}k}<0$ stands for separation. C_{H} is the coefficient of the normal contact stiffness related to the Hertzian contact condition of the wheel and rail, selected as 1.13×10^{11} N/m$^{3/2}$ [38]. Shen-Hedrick-Elkins' model is adopted as the calculation model of the tangential forces between the wheels and rails [20].

2.2.4. Initial and boundary conditions of the system

The displacements and velocities of the sleepers the ballast bodies are assigned to be always zero at the two ends of the track considered in the calculation. The vertical and lateral displacements of the rail ends are always zero due to the hinged ends. The displacement of the subgrade is assumed to be zero. The initial displacements and velocities of the parts of the vehicle and the track are set to be zero in the vertical and lateral directions. In the longitudinal direction the velocity of the vehicle parts is a constant, namely, the curving speed.

Since the present system contains many differential equations and the detailed derivation of the equations is very tedious, the equations and their detailed derivation were omitted in the present paper. Zhai [38, 39] developed a numerical method specifically to solve the coupled dynamic equations of the railway vehicle and track. The stability, calculation speed and accuracy of the numerical method for solving the equations were also discussed in detail.

2.2.5. Calculation model of wheel-rail contact geometry

In the rolling contact calculation of wheel over rail using Non-Hertzian rolling contact theory by Kalker, it is essential to use the normal distances (normal gap) and the contact angles between the wheel and the rail, h_k and δ_k, as shown in Fig. 1. The wheel/rail contact geometry parameters, including h_k and δ_k, depend on $Y_{\mathrm{w}i}$, $\psi_{\mathrm{w}i}$ and $Y_{\mathrm{r}k}$ for the prescribed sizes of the wheelset and the track. $Y_{\mathrm{w}i}$, $\psi_{\mathrm{w}i}$ and $Y_{\mathrm{r}k}$ are obtained through the dynamics calculation of the vehicle curving, as shown in Fig. 1. In order to find more accurate values of the contact geometry parameters, the method for the wheel-rail contact geometry analysis, discussed in Ref. [31], is further improved.

2.3. Rolling Contact Theory of Wheel and Rail

The normal pressure and the creepage between wheel and rail determine are obtained through the detailed analysis on the vehicle curving using the coupling dynamics model of the vehicle and track. They are used to calculate the contact area of the wheel/rail, contact stresses, stick/slip areas, frictional work density and wear volume in the contact area by using the rolling contact theory by Kalker [30]. Until now Kalker's rolling contact theory of three dimensional elastic bodies is very desirable in the rolling contact analysis of wheel and rail system in elastic region. It was modified [31] and is used in the present analysis. In the calculation of the wheel/rail in rolling contact, each calculation step of the wheel rolling along the rail Δx_1=0.8 mm. A mesh consisting of 21×21 uniform square elements with 0.8×0.8 mm^2 is used to cover the potential contact area of wheel/rail. Through the rolling contact calculation, at the center of any element that is assumed to be element J, the normal pressure p_{3J}, the tangent traction component $p_{\tau J}$ (τ=1, 2) and the total slip component $S_{\tau J}$ between the wheel/rail are known. Subscribes τ=1, 2 indicate the two tangent directions of the contact area which are orthogonal. J indicates the number of the square element, and J ranges from 1 to 441. On the same element p_{3J}, $p_{\tau J}$ and $S_{\tau J}$ is, respectively, regarded as a constant.

2.4. Material Wear Model of Rail

The material wear model in which material loss mass of unit area is proportional to frictional work of unit area reads [32,33]

$$\Delta m(x_{J1}, x_{J2}) = C_w f_w(x_{J1}, x_{J2}) \quad (2)$$

In (2), (x_{J1}, x_{J2}) are the coordinates of the center of element J, $\Delta m(x_{J1}, x_{J2})$, and $f_w(x_{J1}, x_{J2})$ are, respectively, the material mass loss of unit area and the friction work density at point (x_{J1}, x_{J2}), the proportional coefficient C_w=1.0×10^{-9} kg(N·m)$^{-1}$ [40]. Considering $p_{\tau J}$ and $S_{\tau J}$ as constants in square element J, (2) is rewritten as

$$\Delta m(x_{J1}, x_{J2}) = C_w f_w(x_{J1}, x_{J2}) = C_w \mid S_{1J} p_{1J} + S_{2J} p_{2J} \mid \quad (3)$$

After a first passage of the wheel, the depth of wear at the center of element J, on the running surface of rail, is written as

$$w_{3J}^{(1)} = C_w \mid S_{1J} p_{1J} + S_{2J} p_{2J} \mid / \rho \quad (12)$$

where ρ=7.8×10^3 kg·m^{-3}, which is the density of the rail material. After k passages the total wear depth is the sum of each wear depth.

Using the procedure discussed in sections 2.3 and 2.4, the wear volume and contact stresses occurred on the rail running surfaces passed by the 4 wheels of the same bogie are predicted when the half vehicle curving through the prescribed track.

3. NUMERICAL EXAMPLE AND DISCUSSIONS

In the numerical analysis, a great number of the structural parameters are used. Their selection can be found in Refs. [35, 36,38]. The analyzed track location is selected at about the center of the circle curve, as shown in Fig. 4. In Fig. 4 point O is the center of the circle curved track. The axis Y indicates in the right side of the track, X in the forward direction of the vehicle. Through the dynamics analysis, we obtain the displacements, velocities, accelerations, spring and damper forces of the system. Also the forces, creepages and the material weal volume of the wheels and rails can be calculated. Some of the interesting results are shown in the following text, and discussed in detail.

3.1. Effect of Curving Speed

When the vehicle passes over the center of the circle curve at 80, 100, and 120 km/h, respectively, as shown in Fig. 4, the normal loads between wheel 1 and the high rail are, respectively, 55.2 kN, 60.4 kN and 66.8 kN. In this case, the super-elevation h_t is 100 mm, the rail cant α_t is 1/40. The highest curving speed leads to the largest normal load generation. The normal pressures on wheel 1 for the three speeds are illustrated by Fig. 5. In the figure signs A, B and C indicate the cases of 80 km/h, 100 km/h and 120 km/h, respectively. The maximum pressures for the three speeds are, respectively, 882.2 MPa, 1459.1 MPa and 994.9 MPa. It is obvious that the highest curving speed does not correspond to the highest normal pressure, 1459.1 MPa. Figure 6 illustrates the distribution of the corresponding longitudinal creep forces. For the speed of 100 km/h, the maximum density of the longitudinal creep force distribution in the contact area is larger than those of the other two speeds. The corresponding patches between wheel 1 and the high rail for the three speeds are shown in Fig. 7. The contact areas for the three speeds are, respectively, 94.4 mm, 72.8 mm and 103.2 mm. The contact area for the speed of 120 km/h is the largest. Hence, the corresponding normal pressure maximum in the contact area is not the highest despite the normal load is the largest, compared with the other two cases. From Figs. 5 to 7, it is obvious that the contact stresses depend on not only the curving speed but also the contact patch of the wheel and rail. The contact patch

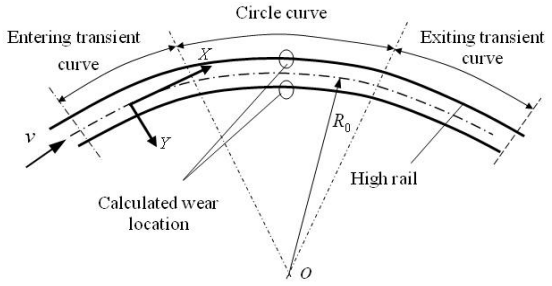

Figure 4. Location of rail wear analyzed on the curved track

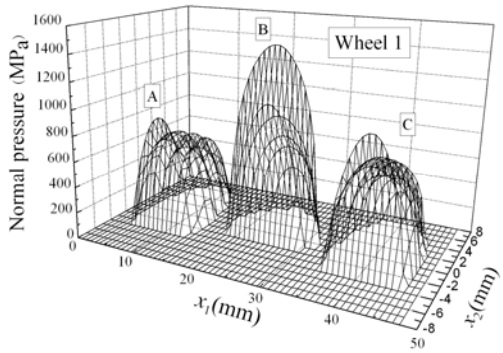

Figure 5. Normal pressures of wheel1 at 80 km/h, 100 km/h and 120 km/h

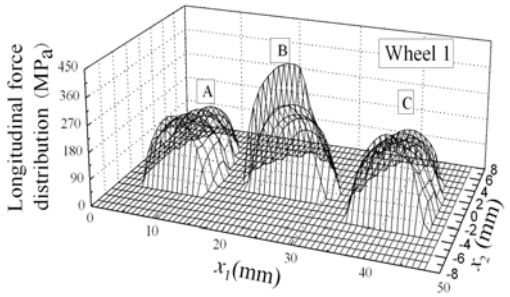

Figure 6. Densities of longitudinal creep forces of wheel 1 at 80 km/h, 100 km/h and 120 km/h

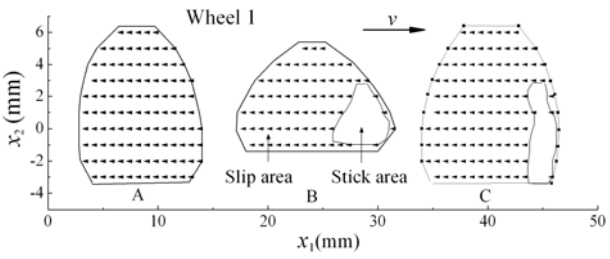

Figure 7. Stick/slip areas of wheel 1 at 80 km/h, 100 km/h and 120 km/h

of wheel/rail relies on the profiles of the wheel/rail and the normal load between the wheel and the rail. Figure 7 shows that the stick area and slip area of wheel 1 are, respectively, 0.0 mm^2 and 94.4 mm^2 at 80 km/h; 11.2 mm^2 and 61.6 mm^2 at 100 km/h; and 9.6 mm^2 and 93.6 mm^2 at 120 km/h. The areas with arrows in Fig. 7 indicate the slip areas, and the empty areas stand for the stick areas in the contact patches. The stick areas exist in the contact patches at 100 and 120 km/h since the normal pressures increase and the total creepages of the wheel and rail decrease. The creepages are not shown in the present paper. Except for the normal load, the contact patch area and its shape also depend on the profiles of the wheel and rail. When the vehicle passes at 100 km/h through the center of the circle curve, the lateral displacement and the yaw angle of the leading wheelset are, respectively, -7.024 mm and 0.058 deg., where the profiles of wheel 1 and the high rail don't match very well. In order to decrease the normal pressure to extend the use life of wheel and rail in service, not only the normal load should be decreased as low as possible but also the profiles should be further optimized. The normal load is concerned with the curving speed and the characters of the vehicle and track. The normal load is reduced by improving the characters of the vehicle and the track. The efficient method for decreasing the normal pressure is to shorten the normal gap formed by the wheel and rail profiles. The smaller normal gap leads to the larger contact area and the lower normal pressure under the condition of the constant normal load. On the other hand, the largely changing the profiles deteriorates the curving behavior of the vehicle probably. Therefore, both the profile change and the superiority curving behavior are simultaneously considered in the improvement of the design of the vehicle and the track. This is a complicated project.

3.2. Effect of Super-elevation of Curved Track and Rail Cant

In the improvement of curving behavior of the vehicle, optimizing the sizes of the track is a good measure. In this section two cases are considered. The first case analyzes the effect of the super elevation h_t on the rail wear and the contact stresses under the condition that the curving speed v =120 km/h, and the rail cant α_t=1/40. The super-elevation of track is defined as the height difference between the out rail and the inner rail of a curved track, and the rail cant angle defined as the slope angle of the rail bottom. The super-elevation h_t is selected as 100, 120 and 140 mm, respectively. In the second case, h_t=120 mm, v=120 km/h, and α_t =1/40, 1/30 and 1/20.

Figures 8, 9 and 10 illustrate the variations of the normal load, the maximum normal pressure and the wear volume, respectively, with increasing h_t. Increasing h_t decreases the reduction in the wheelset loading, as shown in Fig. 8. The maximum normal pressure occurred on wheel 1 goes down and the relatively small normal pressures on the other three wheels go up, as shown in Fig. 9. The wear volumes caused by the 4 wheels have a tendency to decrease with increasing h_t, as shown In Fig. 10. The decrease rate of the wear volume caused

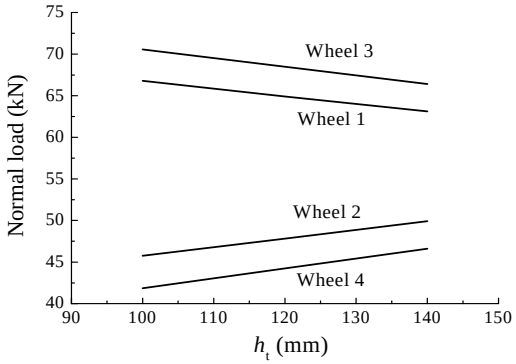

Figure 8. Normal load vs. h_t for v=100 km/h and α_t =1/40

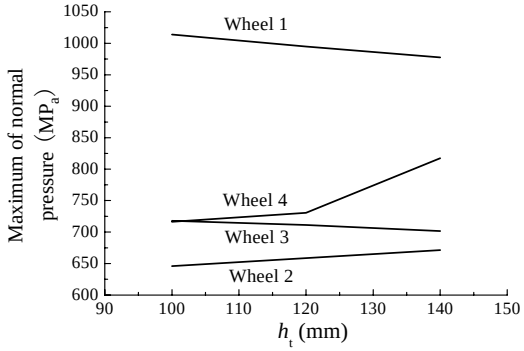

Figure 9. Normal pressure vs. h_t for v=100 km/h and α_t =1/40

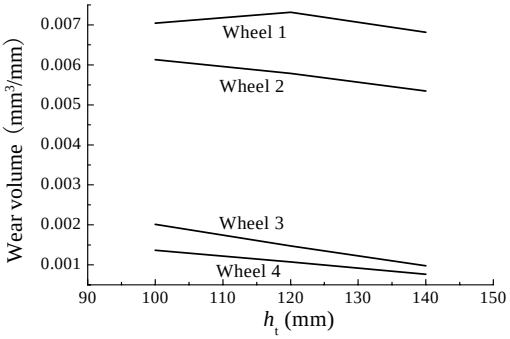

Figure 10. Wear volume vs. h_t for v=100 km/h and α_t =1/40

by wheel 3 is the highest. With h_t increasing the wear rate caused by wheel 1 firstly increases, and then decreases.

Figures 11, 12 and 13 indicate the variations of the normal load, the maximum normal pressure and the wear volume, respectively, with increasing α_t. Figure 11 shows that the reduction in the leading wheelset loading increases and that in the trailing wheelset loading decreases with increasing α_t. When α_t reaches 1/20 the loading reductions of the two wheelsets are almost the same. In increasing α_t the variation amplitudes of the normal loads are not large. Therefore, the effect of rail cant change on the normal loads is very small. But, changing rail cant has a great influence on the normal pressure between wheel 1 and the high rail, as shown in Fig. 12. This is because when α_t equals 1/30, the normal gap formed between wheel 1 and the high curved rail is very large, and

therefore the contact area formed is very small despite the normal load between wheel 1 and the high curved rail does not change much. Increasing α_t decreases the wear volumes caused by wheels 1 and 3, but, sharply increases those caused by wheel 2 and 4, as shown in Fig. 12. Figure 11 shows that the level of the contact stresses at α_t =1/40 is almost the same as that at 1/20. α_t =1/30 is probably a bed choice for this analysis case.

Wheels 1 and 3 roll over the high curved rail, and wheels 2 and 4 roll over the low curved rail. Usually, wheel 1 flange root of the leading wheelset easily contacts the inner gauge cornner of the high curved rail head, and wheel 2 tread easily contacts the field side of the low rail head during the curving. From Fig. 13, increasing rail cant decreases the flange root wear of the wheel on the high curved rail and the wear on the inner gauge corner of the high curved rail, and increases the wear on the field-side tread of the wheel on the low curved rail and the field-side top of the low curved rail. It is because that increasing α_t leads to the contact points between the wheelsets and the pair rails of the track to shift to the field sides.

Based on the results shown in Figs. 8 to 13, and the consideration of the balance in selection of the good behavior and the low contact stresses, it is suggested that α_t =1/40 is selected as the best choice in the rail cant selection for the operation condition of the system considered.

The rail profile change, due to wear, depends on not only the wear volume along the rail running surface but also the wear distribution on the rail top. Figure 14 illustrates the distributions of the rail wear caused by the 4 wheels for the case that v=120 km/h, h_t=120 mm and α_t =1/20. From Fig. 13, the wear volumes caused by wheels 2 and 4 on the low rail are much larger than those caused by wheels 1 and 3, but the widths of their distributions on the low rail top are relatively narrow. The density of the material removal caused by wheel 3 on the high rail is the lowest, but the lateral width of wear is the largest, compared with the other 3 wheels. This is related to the selection of the maximum α_t which changes the contact point positions of the wheels/rails. The wear distribution width depends on the lateral width of the contact area, actually, depends mainly on the wheel/rail profiles at the contact point. At railway sites, if the wear occurring spreads over the rail top uniformly, the use life of the rail can be efficiently extended. At the sharp curved tracks of the heavy haul lines, actually, server wear concentrates on the inside corner of the high curved rail and undulatory wear (corrugation) distributes on the top of the low curved rail. The situation greatly reduces the curving behavior of the vehicle, and causes a strong vibration. So, controlling the rail wear is not only to control the material removal from the rail but also to control its distribution on the rail top.

The wear changes the profiles of the wheel and the rail, and leads to the serious problems discussed above. But, the wear can efficiently eliminate small cracks on the rail running surface, and suppress the growth of the cracks. Based on the principle, railway companies scientifically grind the rails in service to relax the contact stresses, eliminate and reduce the

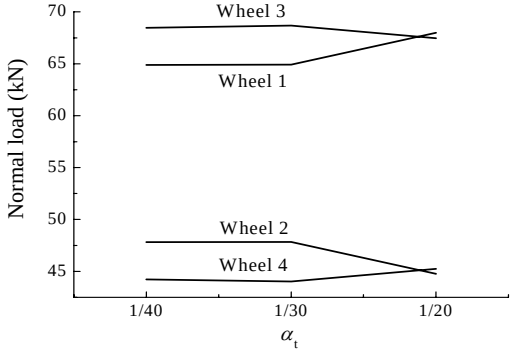

Figure 11. Normal load vs. α_t for v=120 km/h and h_t=120 mm

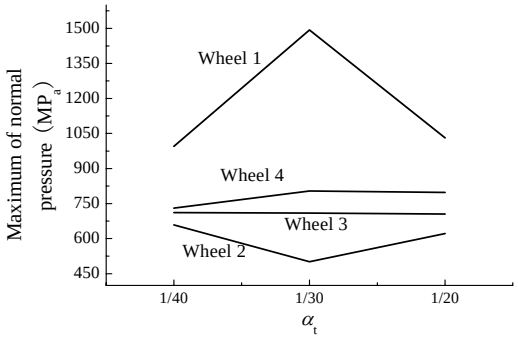

Figure 12. Normal pressure vs. α_t for v=120 km/h and h_t=120 mm

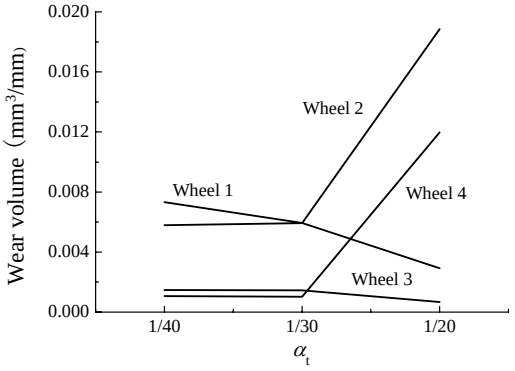

Figure 13. Wear volume vs. α_t for v=120 km/h and h_t=120 mm

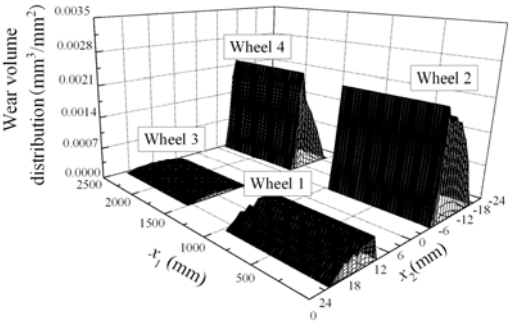

Figure 14. Rail wear distribution on the tops of the rails

rolling contact fatigue of the rails. By the grinding, the profile of the severe wear rail can be renewed. Therefore, the material removal by grinding and its distribution on the rail top is a key technique in the grinding maintenance of track. With the increasing of the natural accumulated wear caused by the repeated rolling/sliding contact of wheel/rail, the continuous change of rail profile will lead to the change of the contact stresses. These are very important problems to be investigated further in the near future.

4. CONCLUSIONS

Some important published papers on wheel-rail wear are reviewed. Their studies are mainly based on laboratory experiments and numerical procedures. Wheel-rail wear study is a very complicated project involving many subjects and many factors some of which are stochastic. Only by test, it is very difficult to identify various factors affecting the wear, and determine how much each contributes to the overall wear and the contact stress level. So far any advanced test facility can't represent track dynamic characters completely, such as non-linear damping and non-linear stiffness. Therefore, the comprehensive theoretical model is essential to clarifying the many factors affecting the curved rail wear and the contact stresses. The present paper investigates the effect of the curving speed, the track super-elevation and the rail cant on the rail wear at the curved track using a numerical method. The numerical results are concluded as follows

(1) The contact stresses between wheel and rail depend on not only the curving speed but also the profiles of the wheel/rail. The curving speed variation leads to the change of wheel/rail normal load and the contact point position. Increasing the curving speed increases the normal loads on the wheels on the high curved rail. But the optimum match of the wheel/rail profiles can form the very small normal gap between the wheel and rail, and efficiently reduces the normal contact stress level increasing due to curving speed increasing. Therefore, the profiles of the wheel and rail dominate the maximum normal contact stress. Therefore the improvement of the profiles is a key technique in reducing the contact stress.

(2) To increase the super-elevation of the curved track properly leads to the improvement of the curving behavior, and the reduction in the contact stresses and the wear.

(3) The rail cant has a great influence on the rail wear and the contact stresses. Changing the rail cant means turning the rail. The contact points on the wheel tread or the rail top shift sharply in the rail turning. In such a situation, the match of the wheel/rail profiles probably becomes more inferior or finer, which depends on the prescribed profiles. Hence, both the selection of the rail cant and the improvement of the wheel/rail profiles should be simultaneously considered in the maintenance of the curved track.

(4) The present paper just investigates the effect of three factors on the curved rail wear and the contact stresses. More factors, such as track gauge, wheel/rail profiles, wheelset geometry sizes, etc., and the crossing influence and the influencing scope of them need to be further investigated.

5. ACKNOWLEDGMENTS

The present work has been supported by National Basic Research Program of China (No. 2007CB714702), the National Natural Science Foundation of China (No. 50521503), the Cultivated Program for Innovative Research Team of Southwest Jiaotong University (No. 2007IRT01) and the Foundation of the Author of National Excellent Doctoral Dissertation of China (2002048).

6. REFERENCES

[1] Clayton, P., 1995, "Predicting the Wear of Rails on Curves From Laboratory Data", Wear, 181-183(1), pp. 11-19.

[2] Wen, Z. F., Jin, X. S., and Zhang, W. H., 2005, "Contact-impact Stress Analysis of Rail Joint Region Using the Dynamic Finite Element Method", Wear, 258(7-8), pp. 1301-1309.

[3] Jergéus, J., Odenmarck, C., Lundén, R., Sotkovszki, P., Karlsson, B., and Gullers, P., 1999, "Full-scale Railway Wheel Flat Experiments", Proc. Inst. Mech. Eng., Part F: J. Rail Rapid Transit, 213(1), pp. 1-13.

[4] Kapoor, A., Fletcher, D. I., and Franklin, F. J., 2003, "The Role of Wear in Enhancing Rail Life", Tribology Research and Design for Engineering Systems, Dowson D. et al., eds., Elsevier B V, pp. 331-340.

[5] Magel, E., Roney, M., Kalousek, J., and Sroba, P., 2003, "The Blending of Theory and Practice in Modern Rail Grinding", Fatigue & Fracture of Engineering Materials & Structures, 26(10), pp. 921-929.

[6] Wu, H. M., Woody, S. S., and Blank, R. W., 2005, "Optimization of Rail Grinding on a North American Haul Railroad Line", Proceedings of the 8th International Heavy Haul Conference, Ronald, J., Costa, L., eds., Brazil, pp. 419-427.

[7] Ishida, M., Abe, N., Moto, T., 1999, "Experimental Study on the Effect of Preventive Grinding on RCF Defects of Shikansen Rails", Proceedings of IHHA'99 STS-Conference, Lisitsyn, A. L., eds., Moscow, Russia, pp. 511-516.

[8] Silva, F. C. M., Vidon, Jr. W., and Caldwell, R., 2005, "Preventive – Gradual On-Cycle Grinding: A First for MRS in Brazil", Proceedings of the 8th International Heavy Haul Conference, Ronald, J., Costa, L., eds., Brazil, pp. 435-445.

[9] Beagley, T. M., 1976, "Severe Wear of Rolling/sliding Contacts", Wear, 36(3), pp. 317-335.

[10] Bolton, P. J., Clayton, P., and McEWEN, I. J., 1980, "Wear of Rail and Tire Steels under Rolling/skidding Conditions", ASLE Transactions, 25(1), pp. 17-24.

[11] Bolton, P. J., and Clayton, P., 1984, "Rolling-sliding Wear Damage in Rail and Tyre Steels", Wear, 93(2), pp.145-165.

[12] Fries, R. H., and Dàvila, C. G., 1985, “Analytical Methods for Wheel and Rail Wear Prediction”, Proceeding of 9th IAVSD Symposium, Linköping, pp. 112-125.
[13] Tyfour, W. R., Beynon, J. H., and Kapoor, A., 1995, “The Steady State Wear Behavior of Pearlitic Rail Steel under Dry Rolling-sliding Contact Conditions”, Wear, 180(1-2), pp. 79-89.
[14] Muster, H., Schmedders, H., Wick, K., and Pradier, H., 1996, “Rail Rolling Contact Fatigue, the Performance of Naturally Hard and Head-hardened Rails in Track”, Wear, 191(1-2), pp. 54-64.
[15] Tournay, H. M., Mulder, J. M. 1996, “The Transition from the Wear to the Stress Regime”, Wear, 191(1-2), pp.107-112.
[16] Ueda, M., Uchino, K., and Kobayashi, A., 2002, “Effects of Carbon Content on Wear Property in Pearlitic Steels”, Wear, 253(1-2), pp. 107-113.
[17] Deters, L., and Proksch, M., 2005, “Friction and Testing of Rail and Wheel Material”, Wear, 258(7-8), pp. 981-991.
[18] Telliskivi, T., and Olofsson, U., 2004, “Wheel-rail Wear Simulation”, Wear, 257(17), pp. 1145-1153.
[19] Shen, Z. Y., and Hedrick, J. K., 1992, “The Influence of Rail Lubrication on Freight Car Wheel/rail Wear Rates”, Proceeding of the International Conference on Rail Quality and Maintenance for Modern Railway Operation, Kalker, J. J., eds., Delft, The Netherlands, pp. 523-535.
[20] Shen, Z. Y., Hedrick, J. K., and Elkins, J. A., 1984, “A Comparison of Alternative Creep-force Models for Rail Vehicle Dynamic Analysis”, Proc. 8th IAVSD Symp., Hedrick J. K., eds., Swets and Zeitlinger, Lisse, pp. 591-605.
[21] Jendel, T., 2002, “Prediction of Wheel Profile Wear-Comparisons with Field Measurements”, Wear, 253(1-2), pp. 89-99.
[22] Archard, J. F., 1953, “Contact and Rubbing of Flat Surfaces”, J. Appl. Phys., 24, pp. 981-988.
[23] Podra, P., and Andersson, S., 1997, “Wear Simulation with the Winkler Surface Model”, Wear, 207(1-2), pp.79-85.
[24] Telliskivi, T., and Olofsson, U., 2004, “Simulation of Wear in a Rolling Sliding Contact by a Semi-Winkler Model and Archards Wear Law”, Wear, 256(7-8), pp. 817-831.
[25] Telliskivi, T., and Olofsson, U., 2000, “Contact Mechanics Analysis of Measured Wheel-rail Profiles Using the Finite Element Method”, J. Rail Rapid Transit, 215, pp. 65-72.
[26] Olofsson, U., and Telliskivi, T., 2003, “Wear, Plastic Deformation and Friction of Two Rail Steels—a Full-Scale Test and a Laboratory Study”, Wear, 254(1-2), pp. 80-93.
[27] Enblom. R., and Berg, M., 2005, “Simulation of Railway Wheel Profile Development due to Wear-influence of Disc Braking and Contact Environment”, Wear, 258(7-8), pp. 1055-1063.
[28] Magel, E., Kalousek, J., and Caldwell, R., 2005, “A Numerical Simulation of Wheel Wear”, Wear, 258(7-8), pp. 1245-1254.
[29] Shevtsov, I. Y., Markine, V. L., and Esveld, C., 2005, “Optimal Design of Wheel Profile for Railway Vehicles”, Wear, 258(7-8), pp. 1022-1030.
[30] Kalker, J. J. 1990, Three-Dimensional Elastic Bodies in Rolling Contact, Kluwer Academic Publishers, Dordrecht, 1990, pp.137-184.
[31] Jin, X. S., Wen, Z. F., Zhang, W. H., and Shen, Z. Y., 2005, “Numerical Simulation of Rail Corrugation on Curved Track”, Computer and Structure, 83(25-26), pp. 2052-2065.
[32] Nielsen, J. B., 1997, “A Nonlinear Wear Model”, ASME, Rail Transportation, RTD-13, pp. 7-20.
[33] Clayton, P., 1996, “Tribological Aspects of Wheel-rail Contact: A Review of Recent Experimental Research”, Wear, 191(1-2), pp.170-183.
[34] Zhai, W. M., Cai, C. B., and Guo, S. Z., 1996, “Coupling Model of Vertical and Lateral Vehicle/Track Interactions”, Vehicle System Dynamics, 26(1), pp. 61-79.
[35] Jin, X. S., Wen, Z. F., Wang, K. Y., Zhou, Z. R., Liu, Q. Y., and Li, C. H., 2006, “Three-dimensional Train-track Model for Study of Rail Corrugation”, Journal of Sound and Vibration, 293(3-5), pp. 830-855.
[36] Jin, X. S., Wen, Z. F., Wang, K. Y., and Xiao, X. B., 2006, “Effect of Passenger Car Curving on Rail Corrugation at a Curved Track”, Wear, 260, pp. 619-633.
[37] Sato, Y., Odaka, T., and Takai, H., 1987, “Theoretical Analysis on Vibration of Ballasted Track”, Railway Technical Research Report, Vol. 1347(1987).
[38] Zhai, W. M., 2001, Coupling Dynamics of Vehicle-Track, China Railway Press, Beijing. (in Chinese)
[39] Zhai, W. M., 1996, “Two Simple Fast Integration Methods for Large-scale Dynamic Problems in Engineering”, International Journal for Numerical Methods in Engineering, 39(24), pp. 4199-4214.
[40] Igeland, A., and Ilias, H., 1997, “Rail Head Corrugation Growth Predictions Based on Non-linear High Frequency Vehicle/track Interaction”, Wear, 213(1-2), pp. 90-97.

